

AEROELASTIC INSTABILITY OF AIRCRAFT WINGS MODELED AS THIN-WALLED COMPOSITE BEAMS

Seher Durmaz* Metin O. Kaya†
Istanbul Technical University
Istanbul-Turkey

ABSTRACT

This study reports static and dynamic aeroelastic analyses of an aircraft wing in an incompressible flow. A swept thin-walled composite beam with a biconvex cross-section is used as the structural model that incorporates a number of non-classical effects such as material anisotropy, transverse shear deformation and warping restraint. A symmetric lay-up configuration *i.e.* circumferentially asymmetric stiffness (CAS) is further adapted to this model to generate the coupled motion of flapwise bending-torsion-transverse shear. For this beam model, the unsteady aerodynamic loads are expressed using Wagners function in the time-domain as well as Theodorsen function in the frequency-domain. The divergence and flutter speeds are evaluated for several ply angles and the results are consistent with the literature, such that the divergence speed is determined to be the most critical speed for forward sweep configurations. The effects of transverse shear, fiber-orientation and sweep angle on divergence and flutter instabilities are further discussed.

INTRODUCTION

There has been a growing interest in the development of the theory of thin-walled composite beams and of their incorporation in various structures ranging from aeronautical/aerospace, automotive, helicopter and turbo-machinery rotor blades, mechanical, civil to naval constructions in the last two decades (Librescu, L. and Ohseop, S. [2006]). From a historical point of view, the theory of thin-walled beams goes back to late 1930s. After the World War 2nd advanced efforts were made to this theory by publications of many books related to it (Librescu, L. and Ohseop, S. [2006]; Oden, J. T. [1967]; Gjelsvik, A. [1981]). Several studies concerning linear static and dynamic behavior of thin-walled composite beams of closed cross-section are contained references (Vo, Thuc Phuong and Lee, Jaehong [2008a,b]). Haddadpour, H. and Zamani Z. [2012] recently reported the aeroelastic design of composite wings modeled as thin-walled beams, in which the wing is optimized using a linear spanwise variation of the fiber orientation for maximum aeroelastic instability speed purpose.

This study presents the aeroelastic analysis of an aircraft wing modeled as a thin-walled composite beam. For this purpose, the structural and aerodynamic models are presented and combined to establish the aeroelastic model of the aircraft wing. The static and dynamic aeroelastic analyses are simultaneously performed for the thin-walled composite beam and the obtained results show good consistency with the literature. The influence of directionality property of composite materials, transverse shear on the aeroelastic instabilities are presented.

STRUCTURAL MODEL

A cantilever beam of length L which is fixed at $z = 0$ and free at $z = L$ is considered. The characteristic cross-sectional dimension of the beam and the maximum wall thickness are represented by d and h , respectively.

*Res. Assist. in Aeronautical Engineering Department, Email: durmazseh@itu.edu.tr

†Prof. Dr. in Aeronautical Engineering Department, Email: kayam@itu.edu.tr

The kinematic variables associated with the Cartesian coordinate system of the beam are denoted by the displacements and cross-sectional rotation which are u , v , w and ϕ . The beam model before and after deformation is shown in Figure 1.

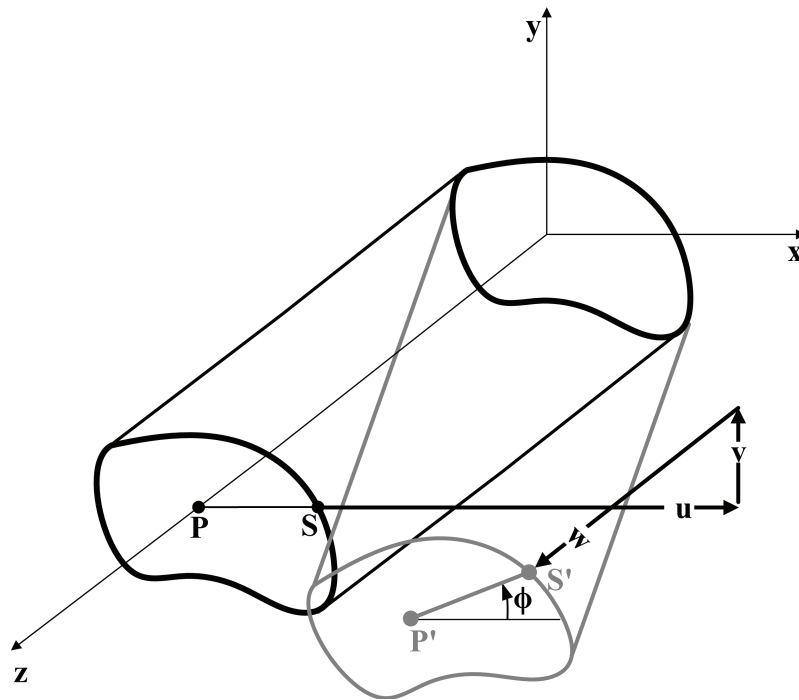


Figure 1: Beam geometry before and after deformation. Point S (before deformation) on the mid-contour moves to S' (after deformation) by translations of u , v and w along x -, y - and z -axes, respectively. ϕ is the rotation of the cross-section.

Displacement Field

In this section, the displacement field of a composite thin-walled beam that undergoes extension, flapwise bending, chordwise bending and torsion deflections is derived. Here, the Cartesian coordinate system is represented by (x, y, z) while the coordinates of the curvilinear system is denoted by (n, s, z_s) . The in-plane translations of point $S(x, y)$ located at mid-contour, are described by u and v .

$$u(x, y, z, t) = u_0(z, t) - y\phi(z, t) \quad (1)$$

$$v(x, y, z, t) = v_0(z, t) + x\phi(z, t) \quad (2)$$

Here, t is time, u_0 and v_0 are the displacements of pole point P , which is located at the origin ($x_P = y_P = 0$) and $\phi(z, t)$ is the rotation of the cross-section. The tangential and normal displacement components associated with the curvilinear coordinate system are u_t and u_n , respectively.

The axial displacement accounting both for primary and secondary warping is given below,

$$w(s, z, t) = w_0(z, t) + \left[y(s) - n \frac{dy}{ds} \right] \theta_x(z, t) + \left[x(s) + n \frac{dx}{ds} \right] \theta_y(z, t) - [F_w(s) - nr_t(s)] \phi'(z, t) \quad (3)$$

The primary warping function accompanied by the quantities off the mid-surface is updated as

$$F_w = \int_C [r_n(s) - \psi(s)] ds \quad (4)$$

Note that the secondary warping function is equivalent to $nr_t(s)$.

Strain Energy

Under the assumption of the cross-section deformability, the strain components ϵ_{ss} , γ_{nn} and γ_{sn} were zero. Thus, the beam cross-sections remain rigid in their own planes. With the non-zero strain components, the

strain energy expression becomes

$$U = \frac{1}{2} \int_0^L \oint_C \int_h [\sigma_{zz} \varepsilon_{zz} + \sigma_{sz} \Gamma_{sz} + \sigma_{nz} \Gamma_{nz}]_{(i)} dndsdz \quad (5)$$

The detailed derivation of strain energy expression is omitted in this extended abstract but it will be covered in the full paper.

Kinetic Energy

The kinetic energy of the beam,

$$K = \frac{1}{2} \int_V \rho_{(i)} (\dot{u}^2 + \dot{v}^2 + \dot{w}^2) dV \quad (6)$$

Inserting the displacements u , v and w into the Eq. 6, we have

$$K = \frac{1}{2} \int_V \rho_{(i)} \left\{ [\dot{u}_P - (Y - y_P) \dot{\phi}]^2 + [\dot{v}_P + (X - x_P) \dot{\phi}]^2 + [\dot{w}_0 + X \dot{\theta}_y + Y \dot{\theta}_x - F_w(s) \dot{\phi}' + nr_t(s) \dot{\phi}']^2 \right\} dV \quad (7)$$

Here, $X = x + n \frac{dy}{dx}$ and $Y = y - n \frac{dx}{dy}$. Expanding the terms in Eq. 7, a very lengthy expression will be obtained. Carrying out the integrations through the wall thickness and around the mid-line contour, reduced mass terms are introduced. This procedure contains a lot of laborious work which was overcome by using parametric programming software, Mathematica.

Work Done by Aerodynamic Loads

The virtual work due to the unsteady aerodynamic loading can be expressed as follows:

$$\delta W_e = \int_0^L [L_{ae}(z, t) \delta v_0(z, t) + M_{ae}(z, t) \delta \phi(z, t)] dz$$

where L_{ae} and M_{ae} are the unsteady aerodynamic lift force and twist moment. They are defined positive in upward direction and nose-up condition, respectively.

STRUCTURAL COUPLING CONFIGURATION

Thin-walled composite beams have extensive usage in many engineering sciences; such as civil, naval and aerospace. The application of the theory varies mostly depending on the geometry of the cross-section, i.e. it is open or closed. The aircraft wing in this study is modeled as a thin-walled composite beam of a single-cell closed cross-section. Due to the composite configuration, different cases of elastic couplings will be exploited. Symmetric configuration also referred as *circumferentially uniform stiffness* (CAS), is adopted to the thin-walled beam presented here, as a result various coupled vibration modes are exhibited. This symmetric configuration is preferred to feature the vertical bending-twist coupling to model the flutter phenomenon. The ply-angle distribution of CAS configuration is displayed in Figure 2. As seen from this figure, the closed cross-section of the thin-walled beam only consists of the top and the bottom walls. On the other hand depending on the geometry, in addition to the top and the bottom walls, the lateral walls may also be included, i.e. rectangular cross-section. In the CAS configuration the ply angle distribution θ is an odd function of spanwise coordinate y , which yields that the following stiffness quantities in the top $(.)^T$ and bottom $(.)^B$ layers appear with a negative sign. This type of beam features two sets of independent couplings: *i*) extension-chordwise bending-chordwise transverse shear coupling, *ii*) flapwise bending-flapwise transverse shear-twist coupling. As mentioned, due to the interest of the present problem the second set of coupling is employed in this study.

AERODYNAMIC MODEL

Theodorsen developed a theory of unsteady aerodynamics for an oscillating thin airfoil in 1934. The lift and the pitching moment at aerodynamic center are expressed by

$$L_{ae} = C_{L\alpha} \rho_\infty U_n b C(k) [-\dot{v}_0 + U_n \dot{\phi} + b \left(\frac{1}{2} - a\right) \dot{\phi}] + \pi \rho_\infty b^2 (-\dot{v}_0 + U_n \dot{\phi} - ba \ddot{\phi}) \quad (8)$$

$$M_{ac} = -\pi \rho_\infty b^3 \left[-\frac{1}{3} \dot{v}_0 + U_n \dot{\phi} + b \left(\frac{1}{8} - \frac{a}{2}\right) \dot{\phi}\right] \quad (9)$$

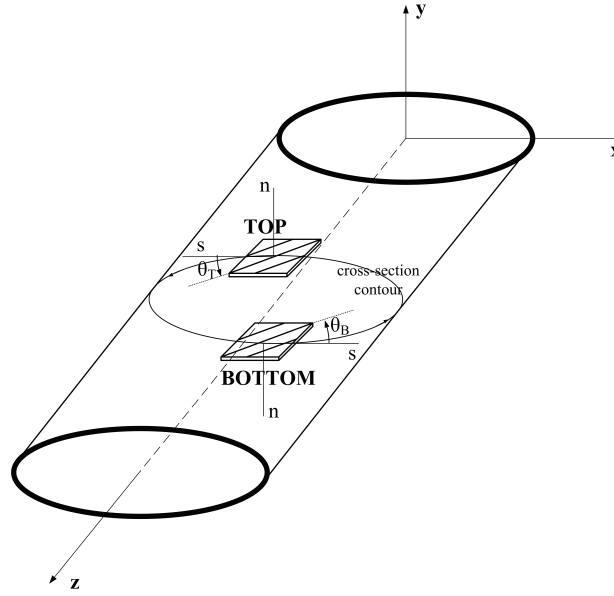


Figure 2: Lay-ups in circumferentially asymmetric stiffness configuration (CAS).

where $()'$ and $\dot{()}$ denote the partial differentiation with respect to the spanwise coordinate along the elastic axis y and reduced time $\tau = U_n t / b$, respectively. U_n is the free stream speed normal to the leading edge, $C_{L\alpha}$ is the lift curve slope and equal to 2π for thin-airfoil theory. v_0 and ϕ represent the plunge displacement and pitch angle of the beam. Here, the function $C(k)$, known as Theodorsen's function, is a complex valued function of reduced frequency k in terms of Hankel functions. It is given by

$$C_k = \frac{H_1^{(2)}(k)}{H_1^{(2)}(k) + iH_0^{(2)}(k)} \quad (10)$$

The twisting moment along elastic axis is expressed as

$$M_{ea} = M_{ac} + \frac{b}{2} L_{ac} \quad (11)$$

Eventhough the Theodorsen theory is appropriate for classical flutter analysis, several situations need an alternative approach such as active flutter control, determination of modal damping in subcritical flight conditions and limit cycle oscillations. One need to express the system in state-space form. To meet these requirements, the aerodynamics loads have to be expressed in terms of the time-domain differential equations. Based on strip theory and $2-D$ incompressible unsteady aerodynamics, the unsteady aerodynamic lift and moment are expressed as follows: the lift and moment expressions of a thin-airfoil for an arbitrary small motion in incompressible flow are given by

$$L_{ae}(z, t) = -\pi\rho_\infty b^2 \dot{w}_{c/2}(z, t) - C_{L\alpha} \rho_\infty U_n b \left[w_{3c/4}(z, 0) \phi_w \left(\frac{U_n t}{b} \right) + \int_0^t \dot{w}_{3c/4}(z, t_0) \phi_w \left[\frac{U_n}{b} (t - t_0) \right] dt_0 \right] \quad (12)$$

$$M_{ae}(z, t) = -\pi\rho_\infty b^3 \left(\frac{1}{2} U_n \dot{\phi} + \frac{1}{8} b \ddot{\phi} \right) - \frac{C_{L\alpha}}{2} \rho_\infty U_n b^2 \left[w_{3c/4}(z, 0) \phi_w \left(\frac{U_n t}{b} \right) + \int_0^t \dot{w}_{3c/4}(z, t_0) \phi_w \left[\frac{U_n}{b} (t - t_0) \right] dt_0 \right] \quad (13)$$

where reduced time is $\tau = \frac{U_n t}{b}$ and $\phi_w(\tau)$ is the Wagner's function which satisfies the expression below,

$$\frac{d\phi_w(\tau)}{d\tau} = \mathcal{L}^{-1}\{C(p)\} \quad (14)$$

where $C(p) = \frac{K_1(p)}{K_0(p) + K_1(p)}$

Here, \mathcal{L}^{-1} is inverse Laplace operator and p is the counterpart of τ in Laplace transformed domain. The generalized Theodorsen function $C(p)$ is described in terms of second kind of modified Bessel's functions (Qin, Z. [2002]; Gulcat, U. [2010]).

To cast the unsteady aerodynamic loads to state-space form, the quasi polynomial approximation is assumed as here reduced time is $\tau = \frac{U_n t}{b}$ and $\phi_w(\tau)$ is the Wagner's function which satisfies the expression below,

$$\phi_w(\tau) = 1 - \sum_{i=1}^n \alpha_i e^{-\beta_i \tau} \quad (15)$$

An explicit expression of Wagner's function does not exist although at subsonic speeds Jones approximation can be used. It suggests a two term approximation with the coefficients $\alpha_1 = 0.165$, $\beta_1 = 0.041$ and $\alpha_2 = 0.335$, $\beta_2 = 0.320$. According to Equations 12 and 13, the terms in square brackets are associated with the circulatory part of the aerodynamic loads and here the Duhamel integral is rewritten as

$$D(z, t) = \int_0^t \dot{w}_{3c/4}(z, t_0) \phi_w \left[\frac{U_n}{b}(t - t_0) \right] dt_0 \quad (16)$$

Inserting Eq. 15 into 16 one gets

$$D(z, t) = w_{3c/4}(z, t) - \sum_{i=1}^n \alpha_i B_i(z, t) \quad (17)$$

where

$$B_i(z, t) = e^{-\beta_i \frac{U_n t}{b}} \int_0^t \dot{w}_{3c/4}(z, t_0) e^{-\beta_i \frac{U_n t_0}{b}} dt_0 \quad (18)$$

Differentiating both sides of the Eq. 18 with respect to time t ,

$$\dot{B}_i(z, t) + \frac{\beta_i U_n}{b} B_i(z, t) = \dot{w}_{3c/4}(z, t) \quad (19)$$

Here, $B_i(z, t)$ are the functions that measure the lag in the induced aerodynamic loads Rodden, W. P. and Stahl, B. [1969]; Qin, Z. [2002]. Thus, instead of evaluating the Duhamel's integral, it is replaced by the equivalent aerodynamic equations of motion given in Eq. 19

Finite-Span Effects

The previous derivation were performed using 2-D aerodynamic theory and the unsteady aerodynamic loads was obtained for an unswept, infinitely long wing. This section points out several modifications made to 2-D aerodynamic model in order to extend it to a 3-D one. Considering swept wings, the unsteady aerodynamic loads are reconsidered to include this effect. To capture finite-span effects the lift curve slope $C_{L\alpha}$ is expressed by involving the corrections to the aspect ratio and sweep angle. The modified expressions are obtained to account the finite-span effects (Bisplinghoff, Raymond L. and Ashley, Holt and Halfman, Robert L. [1996]; Qin, Z. and Librescu, L. [2003]; Qin, Z. [2002]):

$$C_{L\alpha}^{3D} = \frac{2\pi AR}{AR + 2 \cos \Lambda} \quad (20)$$

and

$$\frac{b}{2} \rightarrow \frac{b}{2} \left(\frac{C_{L\alpha}}{\pi} - 1 \right) \quad (21)$$

The unsteady aerodynamic loads given by Eqs. 12 and 13 are updated using Eqs. 20 and 21. If the wing is assumed to be initially at rest, the explicit form of the unsteady aerodynamic loads are obtained in the following.

$$\begin{aligned} L_{ae}(z, t) = & -\pi \rho_{\infty} b^2 [\ddot{v}_0 - U_n \dot{\phi} + U_n \dot{\sigma} \tan \Lambda] \\ & - \frac{C_{L\phi}}{\pi} \rho_{\infty} U_n b \left[\dot{v}_0 - U_n \phi + U_n \sigma \tan \Lambda - \frac{b}{2} \left(\frac{C_{L\phi}}{\pi} - 1 \right) (\dot{\phi} + U_n \chi \tan \Lambda) \right] \\ & + \frac{C_{L\phi}}{\pi} \rho_{\infty} U_n b \sum_{i=1}^n \alpha_i B_i \end{aligned} \quad (22)$$

$$\begin{aligned}
M_{ae}(z,t) = & -\pi\rho_\infty b^3 \left[\frac{1}{2} \left(\frac{C_{L\phi}}{\pi} - 1 \right) (U_n \dot{\phi} + U_n^2 \chi \tan \Lambda) + \frac{1}{8} b (\ddot{\phi} + U_n \dot{\chi} \tan \Lambda) \right] \\
& - \frac{C_{L\phi}}{2\pi} \rho_\infty U_n b^2 \left[\dot{v}_0 - U_n \phi + U_n \sigma \tan \Lambda - \frac{b}{2} \left(\frac{C_{L\phi}}{\pi} - 1 \right) (\dot{\phi} + U_n \chi \tan \Lambda) \right] \\
& + \frac{C_{L\phi}}{2\pi} \rho_\infty U_n b^2 \sum_{i=1}^n \alpha_i B_i
\end{aligned} \quad (23)$$

Recall that the rates of change of bending and twist in spanwise coordinate are $\sigma(z,t) = \frac{\partial v_0}{\partial z}$ and $\chi(z,t) = \frac{\partial \phi}{\partial z}$, respectively.

AEROELASTIC EQUATIONS

In terms of displacement quantities, the governing aeroelastic equations of thin-walled composite beam under flapwise bending-flapwise transverse shear-twist coupling are expressed as

$$a_{55}(v_0'' + \theta_x') - a_{56}\phi''' + L_{ae} = b_1 \ddot{v}_0 \quad (24)$$

$$a_{56}(v_0''' + \theta_x'') - a_{66}\phi'''' + a_{37}\theta_x'' + a_{77}\phi'' + M_{ae} = (b_4 + b_5)\ddot{\phi} - (b_{10} + b_{18})\ddot{\phi}'' \quad (25)$$

$$a_{33}\theta_x'' + a_{37}\phi'' - a_{55}(v_0' + \theta_x) + a_{56}\phi'' = (b_4 + b_{14})\ddot{\theta}_x \quad (26)$$

with the boundary conditions

at $z = 0$:

$$v_0 = \phi = \theta_x = \phi' = 0 \quad (27)$$

at $z = L$

$$a_{55}(v_0' + \theta_x) - a_{56}\phi'' = 0 \quad (28)$$

$$a_{56}(v_0'' + \theta_x') - a_{66}\phi''' + a_{37}\theta_x' + a_{77}\phi' = -(b_{10} + b_{18})\ddot{\phi}' \quad (29)$$

$$a_{33}\theta_x' + a_{37}\phi' = 0 \quad (30)$$

$$a_{56}(v_0' + \theta_x) - a_{66}\phi'' = 0 \quad (31)$$

Here, a_{ij} 's and b_i 's are the elements of stiffness matrix and reduced mass terms. For their expressions one should address to Ref. .

The structural model of the beam of biconvex cross-section had the length of L , width of b and maximum thickness of h and the sketch of it was shown in Figure 3.

SOLUTION METHODOLOGY

To solve the nondimensional aeroelastic equations of thin-walled composite beams, a state space description is required due to nonconservative nature of the eigenvalue problem. Second, using spatial semi-discretization based on Extended Galerkin Method, the governing equations can be expressed in matrix form as follows

$$\left(M_S + \frac{1}{\mu_0} M_{AE} \right) \ddot{q} + \left(\frac{1}{\mu_0} C_{AE} \right) \dot{q} + \left(k_r K_S + \frac{1}{\mu_0} K_{AE} \right) q = \frac{1}{\mu_0} Q \quad (32)$$

where

$$q = \begin{Bmatrix} q_v \\ q_\phi \\ q_x \end{Bmatrix} \quad (33)$$

$$Q = \begin{Bmatrix} Q_v \\ Q_\phi \\ 0 \end{Bmatrix} = \sum_{i=1}^n \alpha_i \frac{C_{L\phi}}{\pi} \begin{Bmatrix} \int_0^1 N_v \hat{B}_i d\eta \\ 0 \\ \frac{1}{2} \int_0^1 N_\phi \hat{B}_i d\eta \\ 0 \end{Bmatrix} \quad (34)$$

Here Θ_v , Θ_ϕ and Θ_x represent the eigenvector matrices with dimension of $N \times m$ and $\Theta = [\Theta_v^T \quad \Theta_\phi^T \quad \Theta_x^T]^T$. Using mode expansion theorem which was explained in Ref. (Meitrovich, L. [1997]; Qin, Z. [2002])

$$q_v = \Theta_v \xi_s \quad q_\phi = \Theta_\phi \xi_s \quad q_x = \Theta_x \xi_s \quad (35)$$

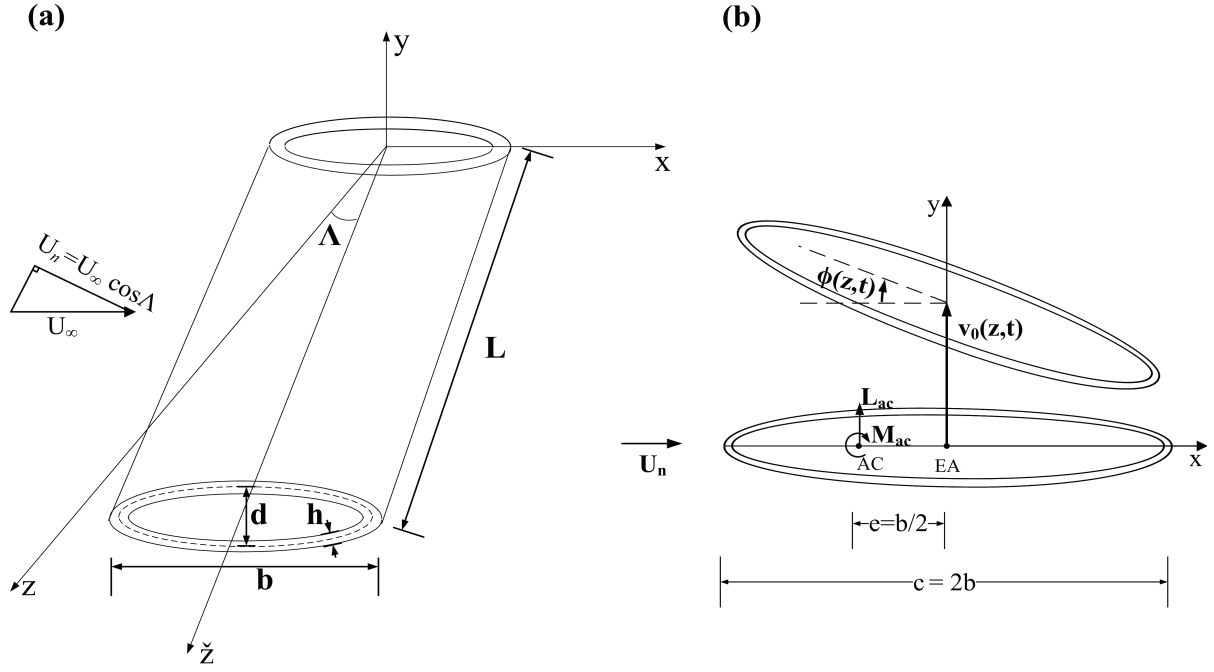


Figure 3: (a) Thin-walled beam geometry. (b) Bi-convex cross-section.

where ξ_s is the vector of first m generalized mode coordinates. Also, M_S , K_S and M_{AE} , K_{AE} denote the mass and stiffness matrices for the structural and aerodynamic models, respectively. The damping is only considered in aerodynamic model.

$$M_S = \int_0^1 \begin{bmatrix} N_v N_v^T & 0 & 0 \\ 0 & I_t N_\phi N_\phi^T + I_w N'_\phi N'^T_\phi & 0 \\ 0 & 0 & r^2 N_x N_x^T \end{bmatrix} d\eta \quad (36)$$

$$K_S = \int_0^1 \begin{bmatrix} \frac{1}{AR^2} N'_v N'^T_v & \frac{a_{56}}{a_{55} L^2 AR} N'_v N'^T_\phi & \frac{1}{AR} N'_v N'^T_x \\ \frac{a_{56}}{a_{55} L^2 AR} N'_\phi N'^T_v & \frac{a_{77}}{a_{55} L^2} N'_\phi N'^T_\phi + \frac{a_{66}}{a_{55} L^4} N''_\phi N''^T_\phi & \frac{a_{37}}{a_{55} L^2} N'_\phi N'^T_x + \frac{a_{56}}{a_{55} L^2} N'_\phi N'^T_x \\ \frac{1}{AR} N'_x N'^T_v & \frac{a_{37}}{a_{55} L} N'_x N'^T_\phi + \frac{a_{56}}{a_{55} L^2} N_x N'^T_\phi & N_x N_x^T + \frac{a_{33}}{a_{55} L^2} N'_x N'^T_x \end{bmatrix} d\eta \quad (37)$$

$$M_{AE} = \int_0^1 \begin{bmatrix} N_v N_v^T & 0 & 0 \\ 0 & \frac{1}{8} N_\phi N_\phi^T & 0 \\ 0 & 0 & 0 \end{bmatrix} d\eta \quad (38)$$

$$C_{AE} = \int_0^1 \begin{bmatrix} \frac{\tan \Lambda}{AR} N_v N_v^T + \frac{C_{L\phi}}{\pi} N_v N_v^T & - \left[1 + \frac{C_{L\phi}}{2\pi} \left(\frac{C_{L\phi}}{\pi} - 1 \right) \right] N_v N_\phi^T & 0 \\ \frac{C_{L\phi}}{2\pi} N_\phi N_v^T & \frac{\tan \Lambda}{8AR} N_\phi N_\phi^T - \frac{1}{2} \left(\frac{C_{L\phi}}{2\pi} - 1 \right) \left(\frac{C_{L\phi}}{\pi} - 1 \right) N_\phi N_\phi^T & 0 \\ 0 & 0 & 0 \end{bmatrix} d\eta \quad (39)$$

$$K_{AE} = \int_0^1 \begin{bmatrix} \frac{C_{L\phi} \tan \Lambda}{\pi AR} N_v N_v^T & \frac{C_{L\phi} \tan \Lambda}{2\pi AR} N_v N_\phi^T - \frac{C_{L\phi} \tan \Lambda}{2\pi AR} \left(\frac{C_{L\phi}}{\pi} - 1 \right) N_v N_\phi^T & 0 \\ \frac{C_{L\phi} \tan \Lambda}{2\pi AR} N_\phi N_v^T & - \frac{C_{L\phi}}{2\pi} N_\phi N_\phi^T - \frac{\tan \Lambda}{2AR} \left(\frac{C_{L\phi}}{2\pi} - 1 \right) \left(\frac{C_{L\phi}}{\pi} - 1 \right) N_\phi N_\phi^T & 0 \\ 0 & 0 & 0 \end{bmatrix} d\eta \quad (40)$$

For simplicity, introducing the following matrices

$$M_n = \Theta^T \left(M_S + \frac{1}{\mu_0} M_{AE} \right) \Theta \quad C_n = \Theta^T \frac{1}{\mu_0} C_{AE} \Theta \quad K_n = \Theta^T \left(k_r K_S + \frac{1}{\mu_0} K_{AE} \right) \Theta \quad (41)$$

The Eq. 36 is rewritten by the help of Eqs. 35 and 41

$$M_n \ddot{\xi}_s + C_n \dot{\xi}_s + K_n \xi_s = \frac{1}{7} \mu_0 \left(\Theta_v^T Q_v + \Theta_\phi^T Q_\phi \right) \quad (42)$$

The right hand side of the Eq. 41 is rewritten in terms of the augmented state vector x_{ai} as follows

$$\Theta_v^T Q_v + \Theta_\phi^T Q_\phi = [\alpha_1 I_{m \times m} \quad \cdots \quad \alpha_n I_{m \times m}] \begin{Bmatrix} x_{a1} \\ \vdots \\ x_{an} \end{Bmatrix} \quad (43)$$

The augmented state vector fulfills the following equation which was given in 19.

$$\dot{x}_{ai} + \beta_i x_{ai} = D_1 \xi_s + D_2 \ddot{\xi}_s \quad (44)$$

where

$$\widehat{D}_1 = \int_0^1 \begin{bmatrix} \frac{C_{L\phi} \tan \Lambda}{\pi AR} N_v N_v^T & -\frac{C_{L\phi}}{\pi} N_v N_\phi^T - \frac{\tan \Lambda}{2\pi AR} \left(\frac{C_{L\phi}}{\pi} - 1 \right) N_v N_\phi^T \\ \frac{C_{L\phi} \tan \Lambda}{2\pi AR} N_\phi N_v^T & -\frac{C_{L\phi}}{2\pi} N_\phi N_\phi^T - \frac{C_{L\phi} \tan \Lambda}{2\pi AR} \left(\frac{C_{L\phi}}{\pi} - 1 \right) N_\phi N_\phi^T \end{bmatrix} d\eta \quad (45)$$

$$\widehat{D}_2 = \int_0^1 \begin{bmatrix} \frac{C_{L\phi} \tan \Lambda}{\pi AR} N_v N_v^T & -\frac{C_{L\phi}}{\pi} N_v N_\phi^T - \frac{\tan \Lambda}{2\pi AR} \left(\frac{C_{L\phi}}{\pi} - 1 \right) N_v N_\phi^T \\ \frac{C_{L\phi} \tan \Lambda}{2\pi AR} N_\phi N_v^T & -\frac{C_{L\phi}}{2\pi} N_\phi N_\phi^T - \frac{C_{L\phi} \tan \Lambda}{2\pi AR} \left(\frac{C_{L\phi}}{\pi} - 1 \right) N_\phi N_\phi^T \end{bmatrix} d\eta \quad (46)$$

$$D_1 = [\Theta_v^T \quad \Theta_\phi^T]_{m \times 2N} \quad [\widehat{D}_1]_{2N \times 2N} \quad \begin{bmatrix} \Theta_w \\ \Theta_\phi \end{bmatrix}_{2N \times m} \quad (47)$$

$$D_2 = [\Theta_v^T \quad \Theta_\phi^T]_{m \times 2N} \quad [\widehat{D}_2]_{2N \times 2N} \quad \begin{bmatrix} \Theta_w \\ \Theta_\phi \end{bmatrix}_{2N \times m} \quad (48)$$

State-Space Representation

The equation given in Eqs. 42 and 44 are cast to space-space form given in compact form as

$$\dot{X} = AX \quad (49)$$

where

$$X = \begin{Bmatrix} x_s \\ x_a \end{Bmatrix}, \quad A = \begin{bmatrix} A_s & B_s \\ B_a A_s & A_a + B_a B_s \end{bmatrix} \quad (50)$$

and

$$A_s = \begin{bmatrix} 0_{m \times m} & I_{m \times m} \\ -M_n^{-1} K_n & -M_n^{-1} C_n \end{bmatrix}_{2m \times 2m} \quad (51)$$

$$B_s = \begin{bmatrix} 0_{m \times nm} \\ \frac{1}{\mu_0} M_n^{-1} [\alpha_1 I_{m \times m} \quad \cdots \quad \alpha_n I_{m \times m}] \end{bmatrix}_{2m \times nm} \quad (52)$$

$$A_a = \begin{bmatrix} -\beta_1 I & \cdots & 0 \\ \vdots & \ddots & \vdots \\ 0 & \cdots & -\beta_n I \end{bmatrix}_{nm \times nm} \quad (53)$$

$$B_a = \begin{bmatrix} D_1 & D_2 \\ D_1 & D_2 \end{bmatrix}_{nm \times 2m} \quad (54)$$

Here, 0 and I show zero and identity matrices with dimensions of $m \times m$. Using a temporal discretization to Eq. 49, we have,

$$X(k+1) = [e^{A\Delta\tau}] X(k) \quad (55)$$

where the discretized transition matrix

$$[e^{A\Delta\tau}] = \sum_{i=0}^{\infty} \frac{A^i}{i!} (\Delta\tau)^i \quad (56)$$

Here, A is the system matrix and $\Delta\tau$ is the sampling time. Solving for $X(k)$, one will extract the generalized coordinate $\xi_s(k)$ and one will finally obtain the aeroelastic response of the aircraft wing. The response functions are

$$\bar{v}_0(\eta, k) = N_v^T(\eta) \Theta_v \xi_s(k) \quad (57)$$

$$\phi(\eta, k) = N_\phi^T(\eta) \Theta_\phi \xi_s(k) \quad (58)$$

$$\theta_x(\eta, k) = N_x^T(\eta) \Theta_x \xi_s(k) \quad (59)$$

Divergence and Flutter Instabilities

The static and dynamic aeroelastic instabilities of swept composite aircraft wings are simultaneously determined using the Eq. 49. Discarding the time derivatives of the unsteady aerodynamics terms, the divergence instability are found via solving the minimum solution of the following equation:

$$\left(k_r K_S + \frac{1}{\mu_0} K_{AE} \right) q = 0 \quad (60)$$

Assuming $X = \bar{X} e^{\lambda \tau}$, the eigenvalue problem which corresponds to flutter condition is expressed as follows

$$(\lambda I - A) \bar{X} = 0 \quad (61)$$

where λ 's are the complex eigenvalues of the system given above. When the real part of λ becomes zero, the imaginary part of the same root corresponds to flutter frequency. This critical state is known as flutter condition.

RESULTS AND DISCUSSIONS

Throughout this section, several results for the thin walled composite beams are presented and discussed. The geometric and material properties of beam models, namely Model A and Model B, are listed in Table 1 (Qin, Z. [2002]; Qin, Z. and Librescu, L. [2003]). Note that Model A is mainly used for flutter analysis, while divergence analysis is carried out for Model B.

Table 1: Material properties and geometric characteristics of the wing.

Material Properties		
E_{11}	206.8 GPa	
$E_{22} = E_{33}$	5.17 GPa	
G_{12}	3.10 GPa	
$G_{13} = G_{23}$	2.55 GPa	
$\nu_{12} = \nu_{13} = \nu_{23}$	0.25	
Density, ρ	1528 kg/m ³	
Geometric Characteristics		
	Model A	Model B
Width, b (m)	0.757	0.259
Depth, d (m)	0.1	0.034
Total thickness, h (m)	0.01	0.0086
Length, L (m)	6.058	3.108
Aspect ratio, $AR = 2L/b$	16	12
Number of layers, N	6	7
Lay-ups	$[\theta]_N$	$[2\theta / -\theta / \theta / 0]_s$

At first, the dynamic analysis is conducted to compute eigenfrequencies and eigenvectors. Subsequently, using the first 5 structural modes and 2 aerodynamic lag terms for each indicial function ($m = 5$, $l = 2$), the static and the aeroelastic analyses are performed to obtain the aeroelastic instabilities.

Static Aeroelastic Analysis

As explained previously, the divergence speeds are calculated and several effects such as transverse shear, ply-angle, aspect ratio on the divergence instability are addressed. It should be kept in mind that the aeroelastic instabilities including divergence and flutter are simultaneously considered by the transient method.

Figure 4 indicates the combined effect of sweep and aspect ratio on divergence instability. Here, each curve represent the variation of divergence speed with respect to aspect ratio ($5 \leq AR \leq 15$) for different sweep angle configurations. These curves are obtained by an increase of 15° in sweep. As seen, the divergence speeds reach to the lowest and the most critical value when (forward) sweep angle is high. The effect of ply angle is also depicted in Figures 4(a) and 4(b) which are plotted for $\theta = 30^\circ$ and $\theta = 45^\circ$, respectively.

Moreover, the effect of ply angle on divergence instability is demonstrated in Figure 5. As seen from this figure, the washin effect for $\theta < 35^\circ - 40^\circ$ yields lower divergence speeds and for $40^\circ < \theta < 90^\circ$, when the washout effect is encountered, the divergence speeds are increased. This was previously reported that swept-forward wings feature the washin/washout effects (Qin, Z. and Librescu, L. [2003]) and to address for these effects one should refer to the coupling stiffness a_{37} .

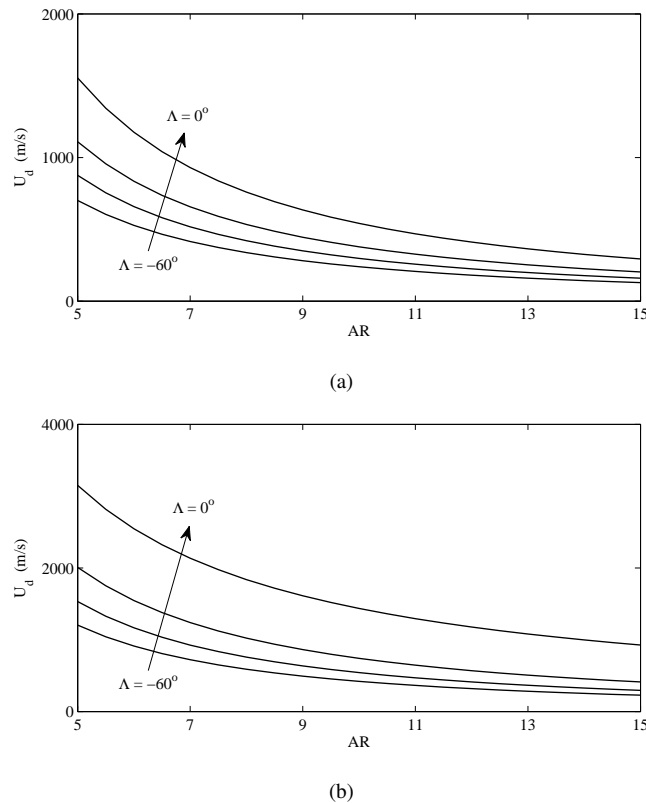


Figure 4: Combined effect of sweep effect of sweep and aspect ratio on divergence speed of Model B for (a) $\theta = 30^\circ$ and (b) $\theta = 45^\circ$.

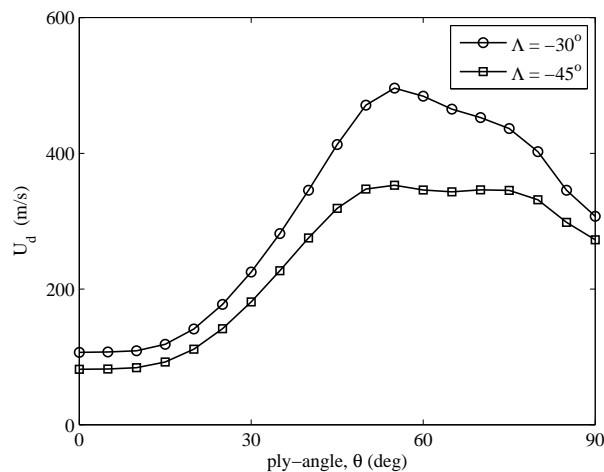


Figure 5: Effect of ply-angle on divergence speed of Model B for $\Lambda = -30^\circ$ and $\Lambda = -45^\circ$

Finally, the static aeroelastic analyses are also performed to illustrate the effect of transverse shear in Figure 6. Here, solid and dashed lines show the results with and without transverse shear, respectively. As seen, when the transverse shear is omitted, the divergence speeds are predicted lower.

Dynamic Aeroelastic Analysis

Test Case:

A computer code is developed in MATLAB to perform flutter analysis and tested with Goland wing. The comparison with several published studies (Durmaz, S. and Ozgumus, O. and Kaya, M. O. [2007]; Patil, Mayuresh J. and Hodges, Dewey H. and Cesnik, Carlos E. S. [2000]; Qin, Z. and Librescu, L. [2003]; Lin, J. and Iliff, K. W. [2000]) is made in Table 2 which shows the flutter speeds in excellent agreement with the

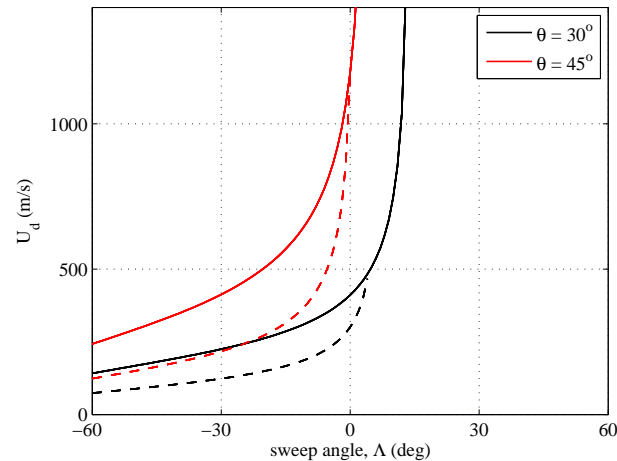


Figure 6: Effect of sweep on divergence speed of Model B for $\theta = 30^\circ$ and $\theta = 45^\circ$.

present predictions.

Table 2: Comparison of flutter results for Goland wing.

Method	U_F (ft/s)	ω_F (rad/s)
Present analysis (EGM)	447	70.1
Durmaz <i>et. al</i> 2007	448	70.3
Patil <i>et. al</i> 2000	445	70.2
Qin and Librescu 2003	450	70.1
Lin and Iliff 2000	447	70.0

Flutter Analysis:

The flutter analyses are also conducted for the thin-walled beam of Model A (see Figure 7). At first, the speeds are calculated by U-g method and transient method, and compared with the published results in Table 3. Here, the results are obtained by taking *i*) $c_{L\alpha} = 2\pi$ and *ii*) $c_{L\alpha} = 2\pi AR / (AR + 2\cos\Lambda)$, which are denoted by superscripts Method^{*i*} and Method^{*ii*}. As seen, finite-span effects play a crucial role in the accurate prediction of the flutter results. Moreover the flutter speeds in both methods (U-g and Transient methods) are in good agreement.

Table 3: Comparison of flutter results calculated by U-g and transient method.

Method ^{<i>i</i>}	U_F (m/s)	ω_F (rad/s)	$U_\infty / (b\omega_{ref})$
U-g method	222.20	89.53	50.70
Transient method	221.60	91.33	50.55
Method ^{<i>ii</i>}	U_F (m/s)	ω_F (rad/s)	$U_\infty / (b\omega_{ref})$
U-g method	234.61	88.20	53.52
Transient method	234.57	89.30	53.52
U-g method Qin, Z. and Librescu, L. [2003]	235.00	87.58	53.74
Transient method Qin, Z. and Librescu, L. [2003]	235.05	87.12	53.75

References

- Haddadpour, H. and Zamani Z. (2012) *Curvilinear fiber optimization tools for aeroelastic design of composite wings*, Journal of Fluids and Structures, Vol 33, p: 180-190, 2012
- Gulcat, U. (2010) *Fundamentals of Modern Unsteady Aerodynamics*, Springer 2010

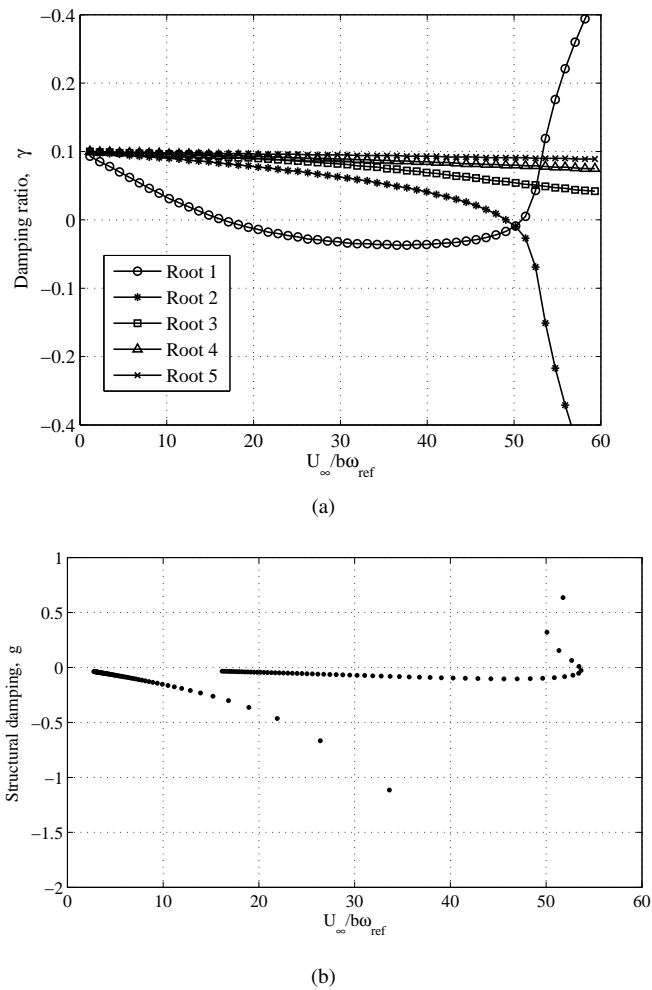


Figure 7: Flutter analysis of Model A (a) by the transient method (b) by U-g method.

- Vo, Thuc Phuong and Lee, Jaehong (2008) *Flexural-torsional behavior of thin-walled composite box beams using shear-deformable beam theory*, Engineering Structures, Vol 30, p: 1958-1968, 2008
- Vo, Thuc Phuong and Lee, Jaehong (2008) *Free vibration of thin-walled composite box beams*, Composite Structures, Vol 84, p: 11-20, 2008
- Durmaz, S. and Ozgumus, O. and Kaya, M. O. (2007) *Aeroelastic analysis of a tapered aircraft wing*, AIAC-2007-109, Ankara International Aerospace Conference, Ankara, Turkey, September 27-29, 2007
- Librescu, L. and Ohseop, S.(2006) *Thin-walled composite beams: Theory and Application*, The Netherlands: Springer 2006
- Qin, Z. and Librescu, L. (2003) *Aeroelastic instability of aircraft wings modelled as anisotropic composite thin-walled beams in incompressible flow*, Journal of Fluids and Structures, Vol 18, p: 43-61, 2003
- Qin, Z. (2002) *Vibration and Aeroelasticity of Advanced Aircraft Wings Modeled as Thin-Walled Beams Dynamics, Stability and Control*, PhD Thesis, Virginia Polytechnic Institute and State University 2002
- Patil, Mayuresh J. and Hodges, Dewey H. and Cesnik, Carlos E. S. (2000) *Nonlinear aeroelastic analysis of complete aircraft in subsonic flow*, Journal of Aircraft, Vol 37, p: 753-760, 2000
- Lin, J. and Iliff, K. W. (2000) *Aerodynamic Lift and Moment Calculations Using a Closed-Form Solution of the Possio Equation*, NASA-2000-209019, 2000
- Meitrovich, L. (1997) *Principles and Techniques of Vibrations*, Prentice-Hall 1997

- Bisplinghoff, Raymond L. and Ashley, Holt and Halfman, Robert L. (1996) *Aeroelasticity*, Dover Publications 1996
- Gjelsvik, A. (1981) *The theory of thin walled bars*, Wiley 1981
- Rodden, W. P. and Stahl, B. (1969) *A Strip Method for Prediction of Damping in Subsonic Wind Tunnel and Flight Flutter Tests*, Journal of Aircraft, Vol 6, p: 9-17, 1969
- Oden, J. T. (1967) *Mechanics of elastic structures*, McGraw-Hill 1967